ChemComm

COMMUNICATION

View Article Online
View Journal | View Issue

Cite this: *Chem. Commun.*, 2022, **58**, 12596

Received 6th August 2022,
Accepted 12th October 2022

DOI: 10.1039/d2cc04401c

rsc.li/chemcomm

Manipulating the inorganic motif by kinetic control of antimony halide organic–inorganic hybrid materials for larger Stokes shift and significantly enhanced quantum efficiency†

Fang Lin,[a] Hua Tong,[b] Haoran Lin [a] and Wei Liu *[b]

Adjusting the structure of the inorganic components has been proved to be an efficient method for the performance optimization of organic–inorganic hybrid materials. One particular organic ligand can typically form numerous hybrid structures with one inorganic source; however, in most cases, only one thermodynamically stable phase can be obtained, which may not be the one with the best properties. Here, we reported a novel method for modulating the optical properties of antimony halide based organic–inorganic hybrid materials by kinetic control of the synthesis. Under such an approach, the kinetically stable phase can be synthesized, which exhibits significantly improved quantum efficiency compared to the thermodynamically stable phase. This approach provides a new route for the development of high-performance organic–inorganic hybrid materials.

Organic–inorganic hybrid materials are composed of both inorganic motifs and organic ligands, and the two components are connected by chemical bonding.[1–3] Since there are inorganic species and organic species in these structures, these materials not only show the optical, electrical and magnetic properties of the original inorganic semiconductor materials, but also have the flexibility and tunability of the organic ligands.[4] And the integration of the two components would lead to the formation of new properties.[5–7] In the past few decades, many hybrid material systems have been developed, and their optoelectronic properties have been thoroughly explored, which has become a research hotspot in the field of new energy materials.[8–13] The application of hybrid materials in the field of energy-saving solid-state-lighting (SSL) requires these materials to have high luminescence efficiency.[14] However, the development of strongly luminescent hybrid materials with quantum efficiency comparable to the efficiency of commercial phosphors remains a challenge.[15–19]

The kinetic control of chemical reactions makes it possible to isolate metastable substances with properties different from those of thermodynamically stable phases.[20] For the synthesis of organic–inorganic hybrid materials, we often observed the formation of different phases during the reaction process. However, these metastable phases may transform into stable ones during the crystal growth process. Therefore, only the thermodynamically stable phase is obtained during hydrothermal or solvothermal reactions, and this phase may not be the one with the best properties. Here, by using kinetic control during the synthesis of antimony halide based organic–inorganic hybrid materials, we successfully isolated a new phase, $H_3(L)_3SbCl_5{\cdot}Cl$ (**1**, where L = 2-(3-methyl-1*H*-imidazol-3-ium-1-yl)acetate), which is different from the phase $H_3(L)_6SbCl_6$ (**2**) obtained by the typical solvothermal method using the same organic ligand and solvents. The structure and luminescent properties of compound **2** were reported in earlier work.[21] Compound **1** emits strong yellow light under UV excitation with an impressively high internal quantum yield (IQY) of 99%, significantly higher than the IQY of compound **2** (73%), and also higher than the IQYs of common commercial phosphors, such as YAG, BAM, and CAT.[22]

Typical solvothermal synthesis from $SbCl_3$, 1-carboxymethyl-3-methylimidazolium chloride and acetonitrile in a 20 mL Teflon-lined stainless-steel autoclave leads to the formation of compound **2**, which is an efficient green-emitter with an IQY of 73%. However, a tiny portion of the powdery sample emitting very bright yellow light was mixed in the products for certain batches of reactions for compound **2**. In order to isolate the yellow-emitting phase, we modified the reaction conditions to heating and refluxing the reactants in a round bottom flask. In this way, we can observe the reaction process and isolate the products immediately when the products form. The $SbCl_3$ and 1-carboxymethyl-3-methylimidazolium chloride in acetonitrile were heated and refluxed under the protection of argon gas.

[a] *Hoffmann Institute of Advanced Materials, Shenzhen Polytechnic, 7098 Liuxian Bl., Shenzhen 518055, Guangdong, P. R. China*
[b] *School of Chemical Engineering and Technology, Sun Yat-sen University, Zhuhai 519082, Guangdong, P. R. China. E-mail: liuwei96@mail.sysu.edu.cn*

† Electronic supplementary information (ESI) available: Experimental details, PXRD patterns, and single crystal X-ray diffraction data. CCDC 2190859. For ESI and crystallographic data in CIF or other electronic format see DOI: https://doi.org/10.1039/d2cc04401c

After refluxing for about 6 hours, colorless crystals with yellow emission began to form in the first place as the kinetically stable phase on the wall of the flask and the products were separated as soon as they formed. A few hours later, crystals with green emission started to form quickly as the thermodynamically stable phase at the bottom of the flask. The two types of crystals were collected and washed with ethanol for further characterization. The yellow-emitting crystals were analysed to be compound **1**, while the green-emitting crystals were analysed to be compound **2**.

The crystal structure of compound **1** was determined by single crystal X-ray diffraction (SCXRD) and the results are summarized in Table S1 (ESI†). For compound **1**, as shown in Fig. 2, every Sb^{3+} ion is coordinated with five Cl^- ions, forming a pyramid-like $[SbCl_5]^{2-}$ polyhedron. The pyramids are balanced and separated by organic ligand ions, resulting in a 0D structure. Compound **1** adopts a monoclinic *P*121 space group, where individual $SbCl_5^{2-}$ pyramids are surrounded by the zwitterionic 2-(3-methyl-1*H*-imidazol-3-ium-1-yl)acetate ions. The total structure is charge-balanced by three H^+ and one Cl^-, forming a phase with the formula $H_3(L)_3SbCl_5{\cdot}Cl$. The bond distance between the Sb atom and the apical Cl atom in $SbCl_5^{2-}$ in **1** is 2.40 Å. The bond lengths between the Sb atom and the other four Cl atoms are all between 2.54 and 2.73 Å, which are comparable to those in other $SbCl_5$ structures. No solvent molecules existed in the structure. Compound **2** was reported previously in which the isolated $[SbCl_6]^{3-}$ octahedral units are separated by the organic ligand ions, forming a 0D structure. Selected bond angles and bond lengths are summarized in Tables S2 and S3 (ESI†). The phase purity of the as-made crystals of compound **1** was confirmed by powder X-ray diffraction (PXRD) (Fig. S1, ESI†). The peak positions observed in the PXRD patterns are in good agreement with those simulated from single crystal X-ray data, indicating that a pure phase is obtained (Fig. S1, ESI†). Details of synthesis and characterization can be found in the ESI.†

UV-vis absorption spectroscopy, steady-state photoluminescence spectroscopy and time-resolved photoluminescence spectroscopy were applied to study the photophysical properties of compound **1**. The optical absorption spectrum of compound **1** was collected at room temperature. The band gap of compound **1** was calculated to be 3.26 eV by the Tauc method (Fig. 3a). Judging from the absorption edge of **1**, there is no absorption in the visible light region, which is consistent with the transparent crystal nature under natural light. Under UV light excitation, single crystals of **1** emit intense yellow light (Fig. 1). Upon excitation, the electrons are excited from the valence band to the conduction band, and the radiative recombination of electrons and holes leads to the strong yellow luminescence of the compound. The room-temperature photoluminescence excitation (PLE) and emission (PL) spectra of **1** are displayed in Fig. 3b. The room-temperature PL lifetime decay curve of **1** is shown in Fig. 3c, revealing a long lifetime (τ) range of 4.33 μs by monoexponential fitting, which indicates the phosphorescence nature of this compound. The plots also show that 340 nm is the optimized excitation energy. The Commission Internationale de l'Eclairage (CIE) chromaticity coordinates (Fig. 3d) for the emission were calculated to be (0.44, 0.53). Temperature-dependent photoluminescence spectra of compound **1** show that the luminescence intensity increases as the temperature decreases (Fig. S3, ESI†). The decomposition temperature of compound **1** was analysed to

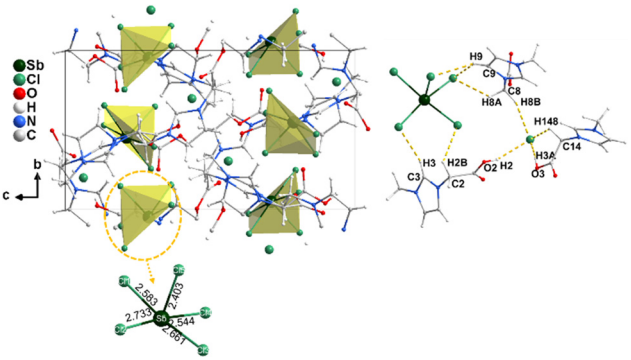

Fig. 2 Structural plot of compound **1**.

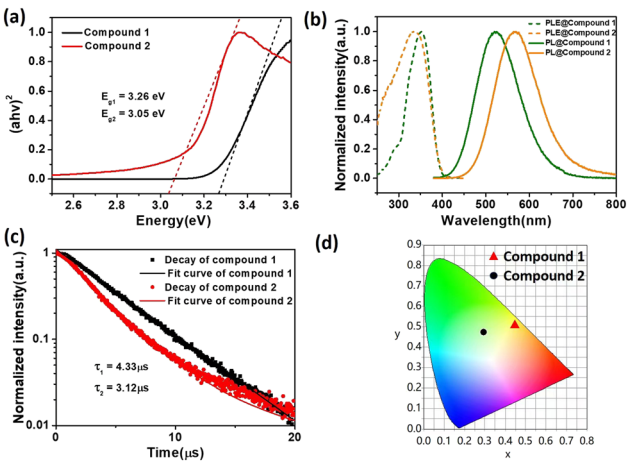

Fig. 3 (a) The Tauc plots of compounds **1** (black) and **2** (red). (b) The excitation spectra (dashed lines) and emission spectra (solid lines) of compounds **1** (green) and **2** (orange). (c) Luminescence decay plots of compounds **1** (black) and **2** (red). (d) CIE coordinates of compounds **1** (red) and **2** (black).

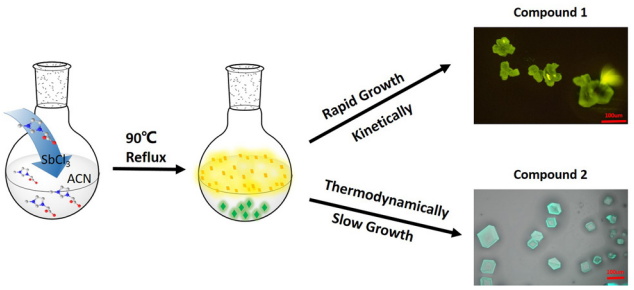

Fig. 1 Synthetic scheme of compound **1** and compound **2** and their crystal morphologies under UV light.

Table 1 Summary of the photophysical properties of 1 and 2

	Compound **1**	Compound **2**
Band gap (eV)	3.26	3.05
Abs_{max} (nm)	340	371
λ_{ex} (nm)	336	351
λ_{em} (nm)	566	525
Emission color	Yellow	Green
CIE coordinates	0.44, 0.53	0.29, 0.48
Stokes shift (nm)	230	174
FWHM (eV)	0.52	0.45
IQY (%)	99	73
τ (μs)	4.33	3.12
λ_{oct}	0.001874	0
σ^2	17.96	2.08

be 180 °C based on the TG plot (Fig. S2, ESI†). The photophysical properties of compound **1** are summarized in Table 1.

Compound **1** shows a large Stokes shift of 230 nm, while the Stokes shift for compound **2** is 174 nm. The larger Stokes shift of compound **1** compared to compound **2** can be explained by the large distortion level of the inorganic motif, which is highly related to the self-trapped exciton (STE) photoluminescence from this type of compound. The distortions of the inorganic anions of these two compounds could be calculated using the equations below:[23]

$$\lambda_{oct} = \frac{1}{5}\sum_{n=1}^{5}\left[\frac{l_n - l_0}{l_0}\right]^2 \quad \text{(five coordinated)}$$

$$\sigma^2 = \frac{1}{7}\sum_{n=1}^{8}\left(\theta_n - 90^\circ\right)^2 \quad \text{(five coordinated)}$$

$$\lambda_{oct} = \frac{1}{6}\sum_{n=1}^{6}\left[\frac{l_n - l_0}{l_0}\right]^2 \quad \text{(six coordinated)}$$

$$\sigma^2 = \frac{1}{11}\sum_{n=1}^{12}\left(\theta_n - 90^\circ\right)^2 \quad \text{(six coordinated)}$$

In these equations, θ_n denotes the bond angle of each Cl–Sb–Cl, l_0 is the average Sb–Cl bond distance, and l_n denotes the individual Sb–Cl bond length. σ^2 and λ_{oct} represent the bond angle variance and bond length distortion level, respectively. The calculation results are listed in Table 1. Both the σ^2 and λ_{oct} values for compound **1** are significantly higher than the values for compound **2**, which gives the explanation for the larger Stokes shift for compound **1**. This also explained the fact that compound **1** has a higher band gap compared to compound **2**, but the emission band for compound **1** is red-shifted compared to compound **2**. Since the ligands for both compounds are identical, their PL variation could be attributed to the difference in the distortion levels of the inorganic motifs.

Density functional theory (DFT) calculations of the density of states (DOS) of **1** were carried out using the CASTEP code implemented in Materials Studio (Fig. 4b). The DOS results showed that the valence-band maximum (VBM) was majorly contributed by Sb 5s orbitals and Cl 3p orbitals, while the conduction-band minimum (CBM) was contributed mostly by

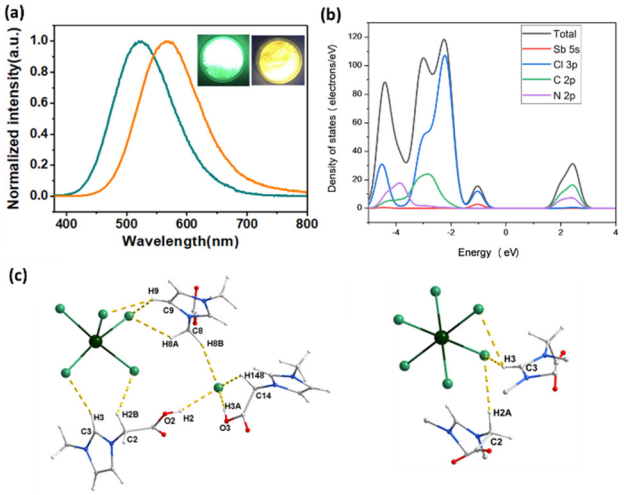

Fig. 4 (a) Emission spectra of compound **1** (yellow) and compound **2** (green), λ_{ex} = 360 nm. Inset: Photos of compound **1** and **2** under UV light irradiation. (b) Density of states plot of compound **1**. (c) Hydrogen bonds of compound 1 (a) and 2 (b). Dark green ball, Sb; green ball, Cl; blue ball, N; red ball, O; grey ball, C; white ball, H.

the organic species (C 2p and N 2p orbitals). The highest occupied molecular orbital (HOMO) was occupied by the inorganic moiety $[SbCl_5]^{2-}$ mostly, while the lowest occupied molecular orbital (LUMO) was occupied by the organic cations. Both the organic and inorganic species would influence the optical properties of compound **1**. The results also show that the band gaps can be systematically tuned by the selection of organic ligands with appropriate LUMO energies. The DOS plot of compound **2** is provided in Fig. S4 (ESI†) for comparison.

The luminescence mechanism of 0D antimony halide hybrid structures has been well-explained by the self-trapped exciton (STE) model.[24,25] Notably, the internal quantum yield (IQY) of compound **1** is as high as 99%, higher than the IQY of compound **2**, and is comparable to the IQYs of commercial phosphors. The luminescence efficiency of these compounds could be influenced by supramolecular interactions such as hydrogen bonding in these structures. The hydrogen bonds in the structures of the two compounds are plotted in Fig. 4c, and we can see that there are more abundant hydrogen bonds among inorganic $[SbCl_5]^{2-}$ anions in compound **1** compared to those of the $[SbCl_6]^{3-}$ anions in compound **2**. The hydrogen bonding details are listed in Tables S3 and S4 (ESI†). The bond angles and distances are different for the two compounds. As for compound **1**, four halide atoms in one $[SbCl_5]^{2-}$ anion form hydrogen bonds with the organic ligands, while for compound **2**, only two halide atoms in one $[SbCl_6]^{3-}$ anion form hydrogen bonds with the ligands. The hydrogen bond number, bond angle and bond length values show that the supramolecular structural rigidity of compound **1** is stronger than that of compound **2**, resulting in weaker nonradiative transition and significant luminescence enhancement.[26]

The origin of the higher photoluminescence quantum efficiency (PLQE) of compound **1** compared to compound **2** can be

Table 2 Comparison of the lifetime values of compounds **1** and **2**

Material	Ave τ (μs)	Ave τ_r (μs)	Ave τ_{nr} (μs)
Compound **1**	4.33	4.37	432.92
Compound **2**	3.12	4.27	11.56

explained by the decay lifetime (τ_r) and nonradiative decay lifetime (τ_{nr}) based on the following equations:

$$\mathrm{PLQE} = \frac{1}{\tau_r} \Big/ \left(\frac{1}{\tau_r} + \frac{1}{\tau_{nr}}\right)$$

$$\frac{1}{\tau} = \frac{1}{\tau_r} + \frac{1}{\tau_{nr}}$$

The calculated τ_r and τ_{nr} values for compound **1** and compound **2** are listed in Table 2. The larger τ_{nr} value for compound **1** compared to compound **2** indicates that the higher PLQE of compound **1** mainly originates from the suppressed nonradiative recombination pathways.[27]

To sum up, a novel method for modulating the optical properties of antimony halide based organic–inorganic hybrid materials by kinetic control of the synthesis was reported. Under such an approach, the kinetically stable phase can be synthesized, which exhibits significantly improved quantum efficiency compared to the thermodynamically stable phase. This approach provides a new route for the controllable synthesis of high-performance organic–inorganic hybrid materials.

F. L. was responsible for performing all experiments and editing the manuscript; H. T. was responsible for the characterization of the compounds and editing the manuscript; H. L. was responsible for reviewing and editing the manuscript; and W. L. was responsible for the supervision of the project, and reviewing and editing the manuscript. All authors gave approval to the final version of the manuscript.

Conflicts of interest

There are no conflicts to declare.

Notes and references

1 K. Chondroudis and D. B. Mitzi, *Chem. Mater.*, 1999, **11**, 3028–3030.
2 D. B. Mitzi, *Progress in Inorganic Chemistry*, John Wiley & Sons, Inc., 2007, pp. 1–121, DOI: 10.1002/9780470166499.ch1.
3 J. Li and R. Zhang, *Progress in Inorganic Chemistry*, John Wiley & Sons, Inc., 2011, pp. 445–504, DOI: 10.1002/9781118148235.ch8.
4 B. Saparov and D. B. Mitzi, *Chem. Rev.*, 2016, **116**, 4558–4596.
5 X. Huang, J. Li and H. Fu, *J. Am. Chem. Soc.*, 2000, **122**, 8789–8790.
6 X. Huang, J. Li, Y. Zhang and A. Mascarenhas, *J. Am. Chem. Soc.*, 2003, **125**, 7049–7055.
7 Z. Yuan, C. Zhou, Y. Tian, Y. Shu, J. Messier, J. C. Wang, L. J. van de Burgt, K. Kountouriotis, Y. Xin, E. Holt, K. Schanze, R. Clark, T. Siegrist and B. Ma, *Nat. Commun.*, 2017, **8**, 14051.
8 J. Wang, N. Wang, Y. Jin, J. Si, Z.-K. Tan, H. Du, L. Cheng, X. Dai, S. Bai, H. He, Z. Ye, M. L. Lai, R. H. Friend and W. Huang, *Adv. Mater.*, 2015, **27**, 2311–2316.
9 Z. Shi, J. Guo, Y. Chen, Q. Li, Y. Pan, H. Zhang, Y. Xia and W. Huang, *Adv. Mater.*, 2017, **29**, 1605005.
10 Q. Zhang, H. Ting, S. Wei, D. Huang, C. Wu, W. Sun, B. Qu, S. Wang, Z. Chen and L. Xiao, *Mater. Today Energy*, 2018, **8**, 157–165.
11 N. Wang, L. Cheng, R. Ge, S. Zhang, Y. Miao, W. Zou, C. Yi, Y. Sun, Y. Cao, R. Yang, Y. Wei, Q. Guo, Y. Ke, M. Yu, Y. Jin, Y. Liu, Q. Ding, D. Di, L. Yang, G. Xing, H. Tian, C. Jin, F. Gao, R. H. Friend, J. Wang and W. Huang, *Nat. Photonics*, 2016, **10**, 699.
12 K. Amnuyswat and P. Thanomngam, *Mater. Today: Proc.*, 2018, **5**, 14857–14861.
13 H. Li, Y. Lv, Z. Zhou, H. Tong, W. Liu and G. Ouyang, *Angew. Chem.*, 2022, **61**, e202115225.
14 J. McKittrick and L. E. Shea-Rohwer, *J. Am. Ceram. Soc.*, 2014, **97**, 1327–1352.
15 C. Zhou, H. Lin, M. Worku, J. Neu, Y. Zhou, Y. Tian, S. Lee, P. Djurovich, T. Siegrist and B. Ma, *J. Am. Chem. Soc.*, 2018, **140**, 13181–13184.
16 L. Mao, P. Guo, M. Kepenekian, I. Hadar, C. Katan, J. Even, R. D. Schaller, C. C. Stoumpos and M. G. Kanatzidis, *J. Am. Chem. Soc.*, 2018, **140**, 13078–13088.
17 L. Mao, Y. Wu, C. C. Stoumpos, B. Traore, C. Katan, J. Even, M. R. Wasielewski and M. G. Kanatzidis, *J. Am. Chem. Soc.*, 2017, **139**, 11956–11963.
18 W. Liu, Y. Fang and J. Li, *Adv. Funct. Mater.*, 2018, **28**, 1705593.
19 W. Liu, W. P. Lustig and J. Li, *EnergyChem*, 2019, **1**, 100008.
20 T. Uemura, in *Kinetic Control in Synthesis and Self-Assembly*, ed. M. Numata, S. Yagai and T. Hamura, Academic Press, 2019, pp. 185–204, DOI: 10.1016/B978-0-12-812126-9.00009-2.
21 F. Lin, H. Wang, H. Lin, W. Liu and J. Li, *Chem. Commun.*, 2021, **57**, 1754–1757.
22 X. Huang, *Nat. Photonics*, 2014, **8**, 748.
23 Y.-C. Peng, Z.-Z. Zhang, Y.-P. Lin, J.-C. Jin, T.-H. Zhuang, L.-K. Gong, Z.-P. Wang, K.-Z. Du and X.-Y. Huang, *Chem. Commun.*, 2021, **57**, 13784–13787.
24 M. Li and Z. Xia, *Chem. Soc. Rev.*, 2021, **50**, 2626–2662.
25 Y. Jing, Y. Liu, M. Li and Z. Xia, *Adv. Opt. Mater.*, 2021, **9**, 2002213.
26 J. Pandidurai, J. Jayakumar, N. Senthilkumar and C.-H. Cheng, *J. Mater. Chem. C*, 2019, **7**, 13104–13110.
27 G. Yu, F. Lin, K. Zhou, S. Fang, Y. Shi, W. Liu, H. Hu, B. Ma and H. Lin, *Chem. Mater.*, 2021, **33**, 5668–5674.